Method to quantify the delocalization of electronic states in amorphous semiconductors and its application to assessing charge carrier mobility of *p*-type amorphous oxide semiconductors

A. de Jamblinne de Meux,[1,2] G. Pourtois,[2,3] J. Genoe,[1,2] and P. Heremans[1,2]
[1]*KU Leuven, ESAT, B-3001 Leuven, Belgium*
[2]*IMEC, Kapeldreef 75, B-3001 Leuven, Belgium*
[3]*Department of Chemistry, Plasmant Research Group, University of Antwerp, B-2610 Wilrijk-Antwerp, Belgium*

(Received 11 September 2017; revised manuscript received 21 December 2017; published 25 January 2018)

Amorphous semiconductors are usually characterized by a low charge carrier mobility, essentially related to their lack of long-range order. The development of such material with higher charge carrier mobility is hence challenging. Part of the issue comes from the difficulty encountered by first-principles simulations to evaluate concepts such as the electron effective mass for disordered systems since the absence of periodicity induced by the disorder precludes the use of common concepts derived from condensed matter physics. In this paper, we propose a methodology based on first-principles simulations that partially solves this problem, by quantifying the degree of delocalization of a wave function and of the connectivity between the atomic sites within this electronic state. We validate the robustness of the proposed formalism on crystalline and molecular systems and extend the insights gained to disordered/amorphous $InGaZnO_4$ and Si. We also explore the properties of *p*-type oxide semiconductor candidates recently reported to have a low effective mass in their crystalline phases [G. Hautier *et al.*, Nat. Commun. **4**, 2292 (2013)]. Although in their amorphous phase none of the candidates present a valence band with delocalization properties matching those found in the conduction band of amorphous $InGaZnO_4$, three of the seven analyzed materials show some potential. The most promising candidate, $K_2Sn_2O_3$, is expected to possess in its amorphous phase a slightly higher hole mobility than the electron mobility in amorphous silicon.

DOI: 10.1103/PhysRevB.97.045208

I. INTRODUCTION

Amorphous semiconductors are an important class of materials for the display industry, as they lie at the heart of the thin-film transistors (TFTs) used in flat-panel display backplanes. Their amorphous nature allows for a uniform deposition of the TFT channel active layer on large areas. The deposition temperature can be low, and compatible with glass and plastic substrates. Despite its low electron mobility less than 1 cm^2/Vs, amorphous silicon (*a*-Si) is still the most commonly used amorphous semiconductor. Recently, amorphous oxide semiconductors (AOS) have attracted much attention with their electron mobility of about 10 cm^2/Vs. In addition to a higher mobility, these materials are also inherently more stable under prolonged electrical bias stress, and have an extremely low off-current [1,2]. For future display applications with high resolution and brightness, there is an urgent demand for even higher charge carrier mobility. Furthermore, there is a trend in display industry to integrate control circuits in the panel with the TFT technology used for the switch matrix. Specifically, the gate drivers that control the selection of the rows in the refresh operation of the display image should be integrated in the panel. As the resolution of the display increases, the required frequency of these gate-in-panel driver circuits increases. This leads to the demand for complementary logic for these circuits, i.e., the existence of both *n*-type and *p*-type transistors. Unfortunately, amorphous oxide semiconductors so far have an extremely low hole mobility, and therefore they do not allow integration of complementary logic circuits.

At present, polycrystalline SnO and CuO are among the most investigated *p*-type oxides semiconductors with a mobility up to ~ 5 cm^2/Vs for high-quality films [3–5]. Unfortunately, the presence of grain boundaries limits the uniformity of the morphology of the film. Since rather high thermal treatments are required ($>350\,^{\circ}C$) to improve their uniformity, these materials are incompatible with plastic substrates or with the complementary metal-oxide semiconductor (CMOS) back-end-of line requirements [6,7]. Furthermore, for *p*-type SnO, it proves nearly impossible to obtain a pure phase in the film: the *n*-type SnO_2 phase is inevitably incorporated simultaneously, which leads to ambipolar behavior and poor leakage currents [8,9]. There is, therefore, a strong need to identify new pure high-mobility amorphous *p*-type materials that can be uniformly deposited on a large area and whose synthesis/deposition is compatible with a lower thermal budget.

Atomistic simulations are powerful tools that provide insights into the electronic properties of crystalline materials and can be used to guide the selection of candidate materials. However, it is complex to use these approaches to predict the mobility of materials, particularly in polycrystalline and amorphous phases. In a crystalline phase, the charge carrier mobility is commonly assessed within Drude's formalism [10,11] based on the evaluation of the effective mass and of the scattering relaxation time. However, the latter requires the quantification of the electron-phonon coupling in the material, which only comes at a high computational cost. Consequently, the screening usually relies on the evaluation of either the conduction or the valence bands effective masses [12–14], assuming that all the materials have an equivalent scattering time.

The problem increases in complexity with polycrystalline or amorphous materials. In case of a polycrystalline materials, the

effective mass remains a valid criterion to qualitatively assess the mobility assuming that the impact of the grain boundaries is sufficiently weak and is equivalent between the different materials under study. However, it is incorrect to justify the use of a crystalline electron or hole effective mass to describe amorphous materials. Indeed, the effective mass concept translates the interaction between atomic orbitals within a periodic crystal potential and hence relies on the information extracted from its first Brillouin zone and the associated band structure. In amorphous phases, the crystal symmetries are nonexistent and, consequently, the concept of band structure ceases to exist. The electronic structure is made of "pockets" of electronic states whose wave functions are more or less delocalized. The extent of this delocalization and the rate at which charges are hopping between the states define the mobility. In the absence of a quantity similar to the effective mass (which reflects the degree of interaction and delocalization of the wave function) for amorphous semiconductors, it is difficult to evaluate the potential of the electronic structure of new amorphous semiconductors using first-principles simulations.

To solve this problem, we propose a methodology to extract the suitability of an amorphous structure to transport holes or electrons. As stated above, the transport mechanism driving these materials is complex: the disordered nature of the atomic structure impacts on the degree of delocalization of the conduction and valence bands and leads to localized electronic states. In the absence of bands, the injected electrons or holes travel using a hopping process between different localized states [15,16]. The displacement of the charge can then be estimated from the knowledge of the distance between the states and the rate at which the electrons hop from one state to the other. As it is possible to compute the hopping rate form Marcus theory [17–19], one could, in theory, evaluate the mobility of these materials. While this approach is popular for organic materials [17,20–22], it is extremely challenging to apply it to the case of inorganic amorphous materials.

A part of the problem originates from the localized nature of the wave function of the electronic states in these disordered materials. In organic semiconductors, charges travel between states that are assumed to be rather well localized on the constituting organic molecules. The "distance" between the states is hence linked to the molecular size, and the hopping rate is approximated from the electronic coupling between states of adjacent molecules.

In an inorganic and amorphous material, the problem is complexified because the distance between the electronic states is *a priori* unknown. In theory, an electronic structure calculation should be able to provide this quantity. But, this requires in practice the use of amorphous models large enough to allow the conduction or valence band states to be fully localized within the model. Given that in a high-mobility material such as amorphous In-Ga-Zn-O (*a*-IGZO), the size of the states easily reaches a few nanometers [23], the size of the cell needed in the simulation is generally too large to be simulated in density functional theory (DFT). Specifically, the dimensions of the unit-cell vectors should be larger than 10 nm, containing more than 10^3 atoms. As a result, it is extremely difficult to study the interaction between the localized states to deduce the electronic coupling between these states, their hopping rates, and hence the mobility. Since it is expected that the mobility will greatly depend on how well the states are delocalized within the amorphous structure, we propose to gauge, in a first-order approximation, the mobility in these disordered systems by how well the conduction or valence band states are delocalized, neglecting the contribution of the coupling.

A well-delocalized electronic state is defined by a wave function that expands over many atoms, forming a continuous path of strongly interacting sites. A well-known electronic population technique used to capture the degree of delocalization of a given state (β) consists in computing the inverse participation ratio (IPR) [24]:

$$\mathrm{IPR}_\beta = \frac{\sum_i C_{\beta i}^4}{\left[\sum_i C_{\beta i}^2\right]^2}, \tag{1}$$

where $C_{\beta i}$ represents the contribution of an atom i in the state β. The IPR values range between zero and one. When all the atoms in a model contribute equally, the IPR reduces to $1/X$, where X is the number of atoms present in the structure, unfortunately leading to a dependence on the model size.

In this paper, we propose a formalism to capture, for a molecular orbital, both the extent and the strength of the interaction between its constitutive atomic orbitals. The formulation and the interpretation of this parameter, the inverse state weighted overlap (ISWO), is discussed in the next section. We study the dependence of the ISWO on the dimension of the model, on the basis set used, and analyze its ability to capture variations in the interactions between atomic sites. The discussion is then broadened to the study of the electronic properties of molecules and crystalline systems to further validate the interpretation of this quantity. Finally, the methodology is applied to disordered materials and used to explore the consequence of disorder on the electronic properties of recently proposed crystalline *p*-type oxide candidates [12].

II. FORMULATION

We formulated the inverse state weighted overlap (ISWO) in the framework of the density functional theory (DFT) based on the expansion of the wave function obtained using a linear combination of atomic orbital (LCAO). All simulations were performed within the CP2K package using a MOLOPT basis set [25,26] and the GTH pseudopotentials [25,27,28]. Unless stated otherwise, the Brillouin zone is sampled in gamma only and double-zeta valence polarized basis sets (DZVP) are used. The exchange correlation was accounted for using the Perdew, Burke, and Ernzerhof (PBE) functional [29]. The *a*-IGZO models accounting up to 189 atoms were generated through the melt and quenching procedure described in [30]. The other amorphous models were generated through a "seed and coordinate" algorithm [31] using the coordination numbers obtained for their crystalline phases available in the material genome project [32–34] as a starting point.

The analysis of the wave-function delocalized character and of the interaction strength between the orbitals finds a natural ground in the LCAO framework. Indeed, a molecular orbital (MO) Ψ_β is expressed in a basis of atomic orbitals φ_{a_i} as $\Psi_\beta = \sum_{a_i} c_{\beta;a_i}\varphi_{a_i}$, where the index a_i corresponds to the index of the atomic orbital i associated to atom a. The amplitude of the bonding character of the wave function between two atomic

sites a and b in a MO is accessed by the analysis of his overlap population $n_{\beta;a,b}$ [35]:

$$n_{\beta;a,b} = 4 \sum_{i,j} c_{\beta;a_i} c_{\beta;b_j} S_{a_i b_j}. \quad (2)$$

The interaction occurring between all the atoms in an MO is then evaluated by summing the $n_{\beta;a,b}$ on all atom pairs. At this stage, it is useful to note that the sign of $n_{\beta;a,b}$ informs on the bonding or antibonding character of the orbital, which is irrelevant for the quantity that we pursue. Consequently, the contribution of the phase is removed by squaring $n_{\beta;a,b}$. Similarly, the constant factor of Eq. (2) is removed, as we intend to quantify the interaction term but not the orbital population. The total interaction between all the atomic sites p_β then takes the form

$$p_\beta = \sum_a \sum_{b<a} \left[\sum_{i,j} C_{\beta;a_i} C_{\beta;b_j} S^2_{a_i b_j} \right], \quad (3)$$

where $C_{\beta;a_i} = c^2_{\beta;a_i}$ are the MO contributions (out of which, the $c_{\beta;a_i}$ are the LCAO coefficients). Note that the sum excludes the unphysical interaction of an atom with itself.

At this stage, the formulation only captures the interaction between the atoms and is rather insensitive to the degree of delocalization of the electronic states. This is corrected in Eq. (4) by introducing in the denominator the maximum value of the atomic contribution of the electronic state of interest ($Mc_\beta = \mathrm{Max}\{\sum_i C_{a_i}\} = \mathrm{Max}\{\sum_i c^2_{a_i}\}$, where $\sum_i C_{a_i}$ sums the contributions of all the orbitals i of an atom a). Indeed, the normalized character of the wave function ensures that a highly localized wave function has a Mc_β value close to one, while a strongly delocalized one has a value close to $1/N$, where N is the number of atomic sites on which the wave function is delocalized. As a consequence, a delocalized electronic state is associated to a large $1/Mc_\beta$ term in Eq. (4), leading to a p_β value larger than 1. Note that the norm of the atomic basis functions is irrelevant for the Mulliken overlap populations and related quantities, i.e., any basis function can be scaled by an arbitrary factor (except zero) without changing the result. We exploit this scaling freedom to require that each atomic basis function is normalized ($S_{ii} = 1$) in order to avoid ambiguities in the following:

$$p_\beta = \sum_a \sum_{b<a} \left[\sum_{i,j} \frac{C_{\beta i} C_{\beta j} S^2_{ij}}{Mc_\beta} \right]_{ab}. \quad (4)$$

Finally, given that the effective mass in periodic structures is inversely proportional to the overlap between the atoms [36,37], the ISWO is defined as

$$\mathrm{ISWO}_\beta = \frac{1}{\sqrt{p_\beta}}, \quad (5)$$

allowing the ISWO_β analysis to remain proportional to the effective mass in simple systems, as demonstrated in the next section. With this definition, a low ISWO value represents a delocalized MO whose atomic orbitals are continuously connected between the different atomic sites, while a high one represents a highly localized and poorly connected MO.

Note that in this formulation, the ISWO is independent of the transport direction being investigated. Such dependence can be introduced by considering that the interaction between two atoms occurs in the direction defined by these atoms. A projection of the ISWO on each Cartesian direction can therefore be obtained by adding a directionally dependent term in the sum, leading to

$$p_{\alpha\beta} = \sum_a \sum_{b<a} \left[\Delta\alpha_{ab} \sum_{i,j} \frac{C_{\beta i} C_{\beta j} S^2_{ij}}{Mc} \right]_{ab} \quad (\alpha = x,y,z), \quad (6)$$

with

$$\Delta\alpha_{ab} = \frac{|R_a(\alpha) - R_b(\alpha)|}{||\boldsymbol{R_a} - \boldsymbol{R_b}||} \quad (\alpha = x,y,z), \quad (7)$$

where the atomic position of an atom α is given by $\boldsymbol{R_\alpha}$. The ISWO value projected in the x, y, or z direction is then obtained by Eq. (5):

$$\mathrm{ISWO}_{\beta\alpha} = \frac{1}{\sqrt{p_{\beta\alpha}}} \quad (\alpha = x,y,z). \quad (8)$$

Nonetheless, the introduction of a directional character into the ISWO [Eq. (8)] leads to consistency issues with Eq. (5), as the latter cannot be recovered from the former. Nevertheless, it still provides a useful insight into the directional patterns in electronic states as presented later in this paper.

III. VALIDATION

To evaluate the capability of the ISWO to provide insightful information on the nature of the interaction between atoms (or orbitals) of a system, we first apply the formalism to periodic systems. In these systems, the electronic states are fully delocalized and the ISWO value provides a measure of the average bond strength between the atom in the considered states. As these should be independent of the dimensions of the model or the basis set used, it is important to ensure that the computed ISWO value converge. Further, given that the ISWO is obtained using the overlap matrix, which reflects the overlaps between the atoms within the unit cell, a sufficiently large number of atoms is required to capture all the non-negligible overlaps in the unit cell.

A. Convergence

In order to gauge the capacity of the ISWO analysis to describe the delocalization of the wave function, the cases of a few simple models are studied. We first consider the case of an ideal linear chain made of hydrogen atoms where the interaction between the atoms is modulated by varying the interatomic distance.

In the case of a hydrogen chain, the ISWO values saturate quickly [see Fig. 1(a)] and five atoms in the unit cell suffice to reach convergence. This suggests that only the first- and second-neighbor interactions are relevant [inset of Fig. 1(a)]. Note that in a more complex material, such as crystalline IGZO [c-IGZO, Fig. 1(c)], the ISWO requires a model with a larger supercell to reach convergence due to the three-dimensional character of the structure and to the integration of the Brillouin zone.

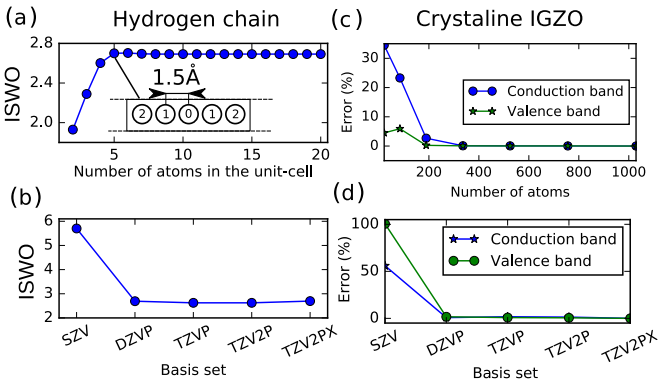

FIG. 1. Convergence of the ISWO computed for a hydrogen chain (a), (b) and for crystalline IGZO (c), (d). (a) The evolution of the ISWO value was computed for the first occupied state of a hydrogen chain as a function of the number of atoms present in the unit cell with a DZVP basis. The hydrogen atoms in the linear chain are distant from 1.5 Å. The inset shows a representation of the five-atom hydrogen model indexed with respect to the central atom (referenced to be 0). (b) Convergence with respect to the size of the basis set for an eight-atom model. (c) Error in % on the ISWO value computed for the conduction and valence bands of *c*-IGZO in function of the number of atoms present in the unit cell. (d) Evolution of the deviation induced by the nature of the basis set for a *c*-IGZO model with 189 atoms. All errors are computed with respect to the value obtained for the most converged simulation. For metals, the largest basis set available is a double-zeta valence polarized (DZVP) one. The triple-zeta valence polarized (TZVP), triple-zeta valence twice-polarized (TZV2P), and triple-zeta valence twice-polarized including *f* orbitals (TZV2PX) labels correspond to simulations where only the basis set of oxygen was increased [26].

For both systems, the ISWO is mostly insensible to the nature of the basis set used as soon as a good quality basis set such as the DZVP one [Figs. 1(b) and 1(d)] is used. A lower-quality basis set tends to overlocalize the electronic states, leading to larger ISWO values.

B. ISWO sensitivity to interatomic interactions

These simple systems are interesting vehicles to modulate the interaction between the atoms. For instance, by increasing the interatomic distance [Fig. 2(a)], the ISWO values can be compared to the calculated effective mass, as illustrated in Fig. 2(a). The relation between the effective mass (m*) and the ISWO values is quasilinear, and illustrates the capacity of ISWO analysis to capture the interaction between the atomic orbitals and their impact on the electronic states.

To probe the capacity of the ISWO analysis to gain directional information, we extended the exercise to anisotropic deformations applied on ideal two-dimensional (2D) and three-dimensional (3D) hydrogen crystals illustrated in Fig. 3.

Similarly to the 1D case, the ISWO values increase in the direction of the deformation [Fig. 4(a)], as illustrated by the impact of a tensile strain applied along the x axis of the hydrogen plane. The ISWO values again follow the evolution of the effective mass [Figs. 4(b) and 4(c)]. In the orthogonal direction, where the distance between the hydrogen atoms is maintained constant, the ISWO values are also increased

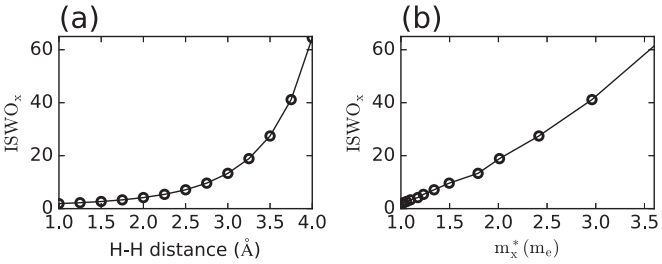

FIG. 2. Variation of the ISWO values for the lowest-energy valence band of the hydrogen chain (a) as a function of the H-H distance and (b) of the effective mass (m*). The effective mass is evaluated using a 1 atom/unit cell and the Brillouin zone was sampled with 10 k points along the chain. The effective mass was then obtained by fitting the bottom of the band with a parabola. In the directions perpendicular to the chain, the unit-cell parameters were set to 8 Å.

but in much weaker proportions. Interestingly, the computed effective mass along this axis remains constant [Fig. 4(c)]. This discrepancy arises from the contribution of the interaction between the atomic sites along the diagonal direction, which also varies with the dilatation of the unit cell. As m* is insensible to this variation, the ISWO values and m* diverge along the y axis. In absence of projections, the ISWO values increase with the deformation to saturate to the value $ISWO_y \approx ISWO$, i.e., whenever the interaction along the x direction becomes negligible. In this asymmetric case, the direction-independent formulation of the ISWO no longer evolves linearly with the averaged effective mass, as shown by the black crosses in Fig. 4(c).

For a 3D cubic hydrogen crystal, the interatomic distance was varied between the hydrogen sites along the two directions (x, y) using asymmetric step sizes (Fig. 3). The results (Fig. 5) are similar to the 2D case: along the directions in which the deformation takes place, the ISWO values are (quasi)linearly correlated to the effective mass. In the one unaffected by the deformation, both ISWO values and effective masses vary slightly [Fig. 5(d)], due to the incomplete projection of the ISWO along the Cartesian axes, as suggested previously.

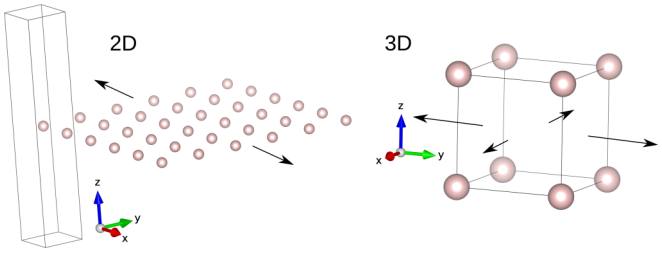

FIG. 3. Representations of an ideal 2D and 3D hydrogen crystal models. The deformations applied to these structures in Figs. 4 and 5 are depicted by arrows. In the 2D case, the deformation is only applied along the x direction. In the 3D one, the deformation is performed along the x and y directions. In both cases, the resulting increases of the bond length span from 1 to 4 Å in the x direction and, in the 3D case, from 1 Å to 2.5 Å in the y one. The atomic structures were rendered with the VESTA package [38].

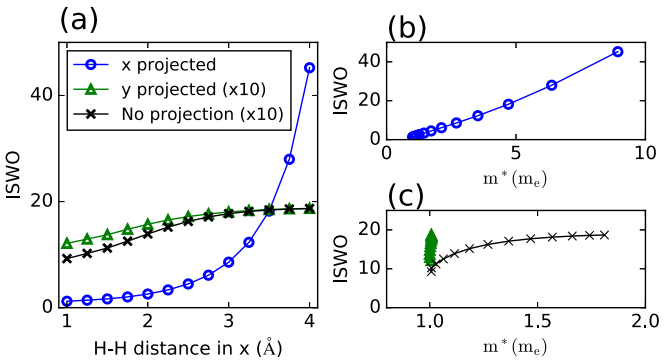

FIG. 4. Variation of the ISWO values computed for the lowest-energy valence band for a 2D hydrogen model containing 100 atoms per unit cell forming the square lattice illustrated in Fig. 3. The distance between the atoms is increased along the x direction, and is kept constant at 1.5 Å in the y direction. (a) Variation of the ISWO values as a function of the H-H distance projected along the x (blue circles) and y (green triangles) directions following Eq. (8), as well as the unprotected ISWO analysis (black cross) as given by Eq. (5). (b), (c) Report the same ISWO evolution with respect to the resulting effective mass (m*). The average effective mass is obtained by the application of a harmonic average along the three Cartesian directions. In the three plots, the blue circles provide the values projected along the x direction, the green triangles along y, and the black crosses indicate the unprotected values [Eq. (5)]. For clarity, the unprotected and y-projected ISWO curves were multiplied by 10.

C. ISWO sensitivity to the electronic interactions

The hydrogen models show that the ISWO metric is able to capture variations of the interatomic interaction in simple cases, which mostly originate from changes in the orbital overlap. But, the ISWO also captures subtle variations in the electronic correlation, even in absence of changes in the overlap. This is exemplified in the case of a crystalline IGZO

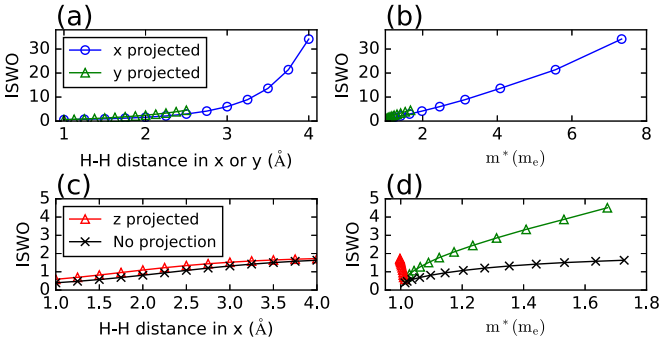

FIG. 5. Variation of the ISWO analysis computed for the lowest-energy valence band state for a cubic bcc stack of hydrogen containing 125 atoms per unit cell (illustrated in Fig. 3). The distance between the hydrogen atomic sites is increased asymmetrically in the x direction by steps of 0.1 Å and by steps of 0.05 Å in the y direction. The distance along z is kept constant at 1.5 Å. (a) Indicates the variation of the ISWO projected in the x and y directions as a function of the H-H bond length in their respective directions. (b) Reports the evolution of the unprotected ISWO values versus effective mass. (c), (d) Provide the same information projected along the z direction and for the unprotected case.

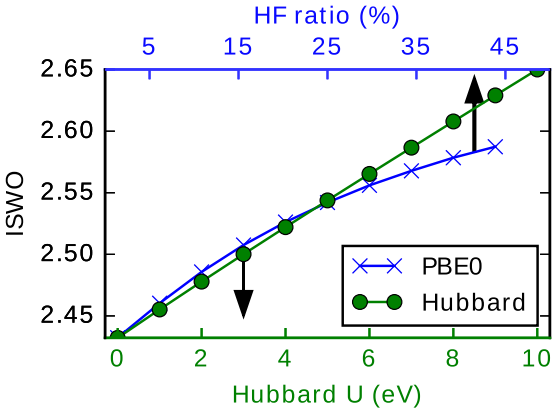

FIG. 6. Variation of the ISWO values computed for the conduction band of crystalline $InGaZnO_4$ as a function of a change of the electronic exchange correlation. This modulation is driven by an increase of the Hubbard term applied to the d orbital of the metals and to the p orbital of the oxygen (green dots) or to the inclusion of a part of Hartree-Fock exchange (blue crosses).

model containing 189 atoms in its unit cell. The electronic correlation was modulated by either tuning the onsite Coulomb interaction (using a Hubbard correction scheme) applied on the d orbitals of the metal cations and on the p orbitals of the oxygen anions or by modulating the amount of Hartree-Fock exchange in a hybrid functional calculation. Both methods only modify the contribution of the electronic exchange correlation and not the overlap since these overlaps are directly obtained from the base functions, which are by definition invariant. As expected, the modification of the exchange correlation increases the localization of the electronic states and hence the ISWO values, as illustrated in Fig. 6. This confirms the ability of the ISWO analysis to reflect variations in the electronic correlation.

D. Validation on crystals and molecules

Figure 7 depicts the variation of the ISWO values for the first valence band state of different carbon allotropes, organic molecules, and for the crystalline phases of silicon, germanium, and tin. The lowest ISWO value is obtained for diamond, where the three-dimensional nature of the wave function allows a complete delocalization on all the atomic sites of the crystal. The ISWO values slightly increase for graphite, bilayer graphene, and monolayer graphene indicating a reduction of the average bonding strength between the carbons due to the absence of direct bonds in the third dimension.

The ISWO values are further enhanced when going to molecules. In organic molecules, the wave function is not as uniformly delocalized as for the carbon allotropes due to the heterogeneous nature of the bonds present in the alkyl molecules, as reflected by the increase in ISWO. As expected, the benzene ring scores lower than the linear chain of carbon in our analysis scheme, due to the π-π interaction present in the delocalized electron cloud of the aromatic ring. Tuning the chemistry of the alkyl chain by substituting a hydrogen atom by a fluorine one leads to a strong localization of the wave function around the fluorine site and to a sharp increase in its ISWO value. The addition of a second fluorine atom breaks the

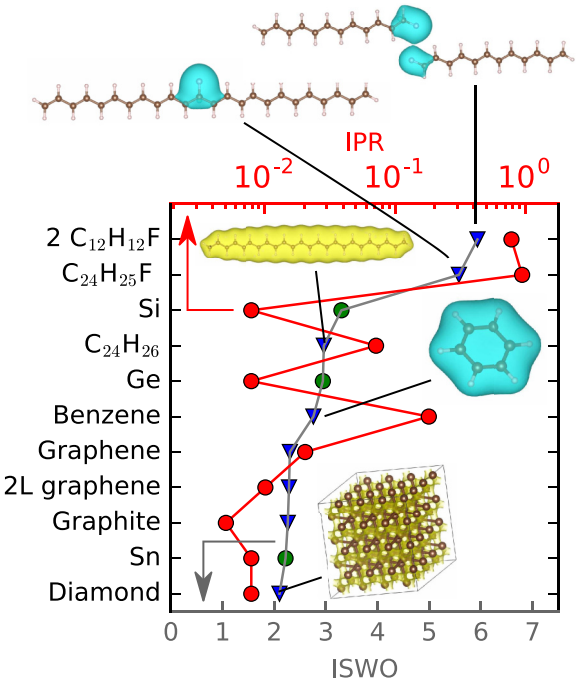

FIG. 7. ISWO and IPR values of the lowest-energy state of graphite, bilayer (2L), monolayer graphene and of some organic molecules (blue triangles) and diamond, bulk silicon, germanium, and tin (green circles). The inset provides the representation of the wave functions of diamond, benzene, and polyethylene ($C_{24}H_{26}$) with and without fluorine and finally of two interacting molecules of fluorinated polyethylene ($C_{12}H_{12}F$) close to each other (rendered with the VESTA [38] package). The wave functions of silicon, germanium, and tin are visually similar to the one of diamond.

symmetry of the chain, leading to a state strongly localized on the two fluorine atoms, which weakly interact with each other. This weak interaction further increases the ISWO, although the localization increases spatially.

The wave functions of the lowest occupied band of diamond, silicon, germanium, and tin have a delocalized signature built from the combination of different s orbitals. However, the lattice dimensions and bond lengths vary strongly from system to system and dominate the ISWO analysis. The smallest value is found for diamond which also owns the shortest and strongest bond. A larger ISWO value is observed for tin, which presents the most delocalized s orbital ($5s$). Germanium and silicon have slightly higher values, indicating the worst tradeoff between the delocalization of their s orbitals and of their bond lengths.

If we set this analysis in perspective with the commonly known use of the inverse participation ration (IPR), we note that the variations of the IPR values are more erratic due their dependence on the number of atoms. For instance, the IPR of $C_{24}H_{26}$ is lower than the one of benzene because the latter owns fewer atoms in its structure. Interestingly, at an equivalent number of atoms, the ISWO and the IPR values can display opposite behaviors. For instance, $C_{24}H_{25}F$ has a larger IPR value than the two interacting $C_{12}H_{12}F$ molecules because more atomic sites are contributing to the wave function of this system than in $C_{24}H_{25}F$. On the contrary, the ISWO analysis provides a different insight and a reverse tendency is observed due to the very weak interaction between the two fluorine atoms of the two distinct molecules. This weak interaction deteriorates the ISWO value and dominates the contribution due to the increase of the wave-function delocalization which should result in an increase of the ISWO value. A parallel can be made with the effective mass in crystalline materials, in which the effective mass also increases when the interaction between the atoms decreases, in line with the fact that strong interatomic interactions are needed to obtain delocalized states.

IV. APPLICATION TO AMORPHOUS STRUCTURES

In crystal phases and molecules, the ISWO analysis provides insights in the atomic and orbital interactions in a specific electronic state. As illustrated in the previous sections, it successfully captures variations of these interactions across different materials and structures. Yet, the intent of the ISWO analysis consists in investigating the properties of amorphous materials and not to focus on either crystalline phases or on molecules, for which more suitable analysis techniques of the electronic structure exist [39]. The ambition of the ISWO is to provide insights in the electronic structure of amorphous materials and to reveal which ones are the most likely to display a high charge carrier mobility in either their valence or the conduction band. We therefore apply the ISWO analysis to the case of amorphous $InGaZnO_4$ (a-IGZO), the best-known n-type "high-mobility" (>10 cm^2/Vs) [40,41] amorphous semiconductor and compared it to amorphous silicon (a-Si), the most common amorphous semiconductor, which presents a much lower charge carrier mobility (<1 cm^2/Vs [40,41]). Since the ISWO only captures the delocalization, it cannot be used to predict the mobility directly. Rather, it is designed to identify disordered semiconductors with the best potential to display a large carrier mobility thanks to their highly delocalized valence or conduction bands.

The distribution of the ISWO analysis obtained for different a-IGZO models is provided in Fig. 8. As the structure of an amorphous material is not uniquely defined, small variations in the ISWO values are natural due to modulations in the atomic configuration used in the models. For the conduction band (green line in Fig. 8), the main contribution originates from highly delocalized s orbitals and we observe that the variability in ISWO values is remarkably small, at the exception of the signature obtained for a model with 315 atoms in which the enhanced localization arises from the contribution of an oxygen p orbital. Interestingly, this exception confirms that, within a defined stoichiometry, the ISWO analysis captures subtle variations in atomistic models. Also, it is worth noticing that, in the present case, the number of atoms considered has almost no impact on the description of the conduction band, confirming that the ISWO values are converged with respect to the dimension of the model used. By contrast, the IPR values are strongly impacted by the size of the model. This is not surprising as, by constructions and in the limit case where the wave function is equally localized on all atoms, the IPR is equals to $1/X$, with X the number of atoms as shown in the Introduction.

In contrast to the signature of the bottom of the conduction band, the ISWO analysis of the top of the valence band reveals

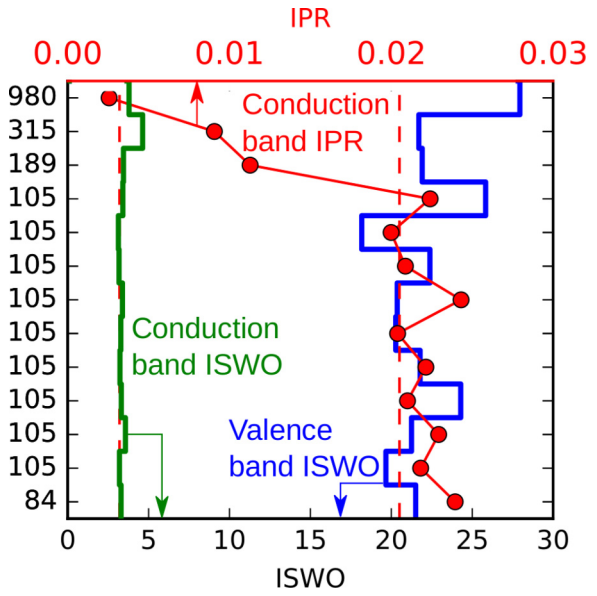

FIG. 8. Comparison of the ISWO and IPR profiles computed for 13 different atomistic models of a-IGZO containing from 84 to 980 atoms. The distribution of the conduction (green) and valence bands (blue) is obtained by averaging the ISWO and IPR values over an energy range of 0.3 eV with respect to the first conduction/valence states to account for the energy window accessible to the charge carriers in a-IGZO transistor [42]. The red dashed lines represent the value of the conduction/valence ISWO averaged for all models.

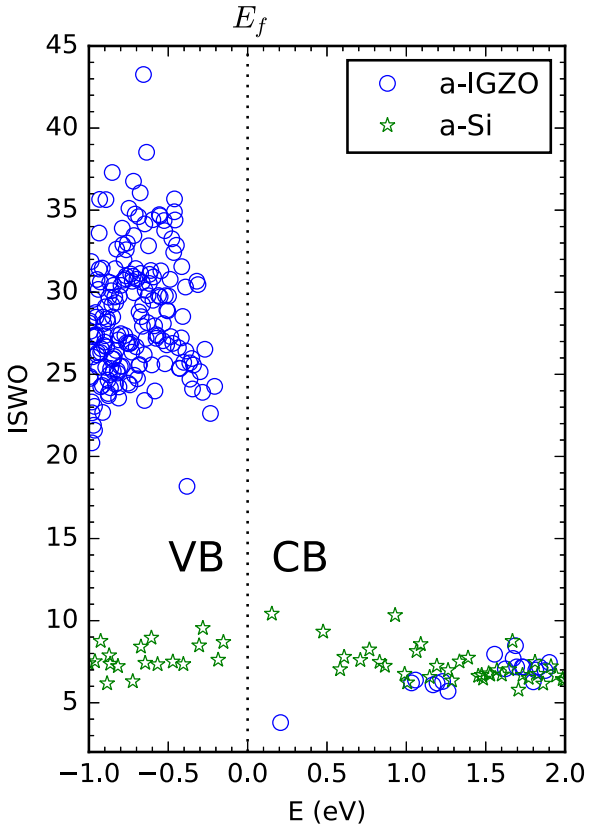

FIG. 9. Evolution of the ISWO as a function of the band energy for an a-IGZO model containing 980 atoms (a) and a model of a-Si (b) with 120 atoms. The dashed vertical lines indicate the position of the Fermi level within the band gap. The band-gap value is highly underestimated due to the use of a semilocal exchange correlation functional (PBE functional [29]). Note that the band gap is further reduced compared to the crystalline phase due to the amorphization process [30].

a strong sensitivity to the specificities of each model (Fig. 8). While the largest model (980 atoms per unit cell) shows the largest ISWO value, there are no correlations between the model size and the ISWO values, indeed, the models with the second largest and the smallest ISWO values both own 105 atoms. The valence band variation finds its root cause in the distribution of the oxygen valence band tail states. Indeed, amorphous materials are typically characterized by localized states tailing deep into the band gap [43,44]. With this respect, a-IGZO is unique since its tail states [42,45] are mainly located close to the valence band. So, while the value of conduction band ISWO is rather independent of the precise model (see Fig. 8), this is not the case for the valence band, which displays a strong variation due to the presence of more or less delocalized band edge states, depending on the model used. This indicates that these electronic states are not suitable for an efficient hole transport process due to their highly localized character.

The localized character of the valence band of a-IGZO is evidenced by the ISWO distribution as a function of the states' energy, as displayed in Fig. 9 (blue circles). For a-IGZO, the distribution is completely different for the conduction band compared to the valence bands. For the former, the ISWO value is stable and decreases while approaching the gap. In the latter, the ISWO values change substantially and tend to increase while approaching the gap, indicating that the states at the top of the valence band are the most localized ones.

For comparison, we also plot in Fig. 9 (green stars) the ISWO values of the valence band and conduction band states of a-Si. Both the conduction and valence bands show variations of the ISWO values and a rather strong localization of the states close to the band gap. Furthermore, we observe that the ISWO values are larger (∼9) than the ones obtained for the a-IGZO conducton band (∼4), implying that a-IGZO has a higher electron mobility compared to a-Si, consistently with experimental observations [46].

From this comparison between a-Si and a-IGZO, we conclude that the value of the ISWO for an ideal high-mobility semiconductor should be as small as possible for the conduction or the valence band, but also be rather constant within the bands accessible to the charge carrier. Finally, the signature should be as independent as possible of the amorphous model used. These requirements are fully met for the conduction band of a-IGZO but not for its valence band, while for a-Si, these conditions are fulfilled neither for the valence nor for the conduction bands.

V. ANALYSIS OF THE PROPERTIES OF p-TYPE OXIDE SEMICONDUCTORS CANDIDATES

As stated previously, a low ISWO value for the top of the valence band states hints to the presence of delocalized electronic states and a signature of a high p-type mobility. We investigate the evolution of the properties upon amorphization of a set

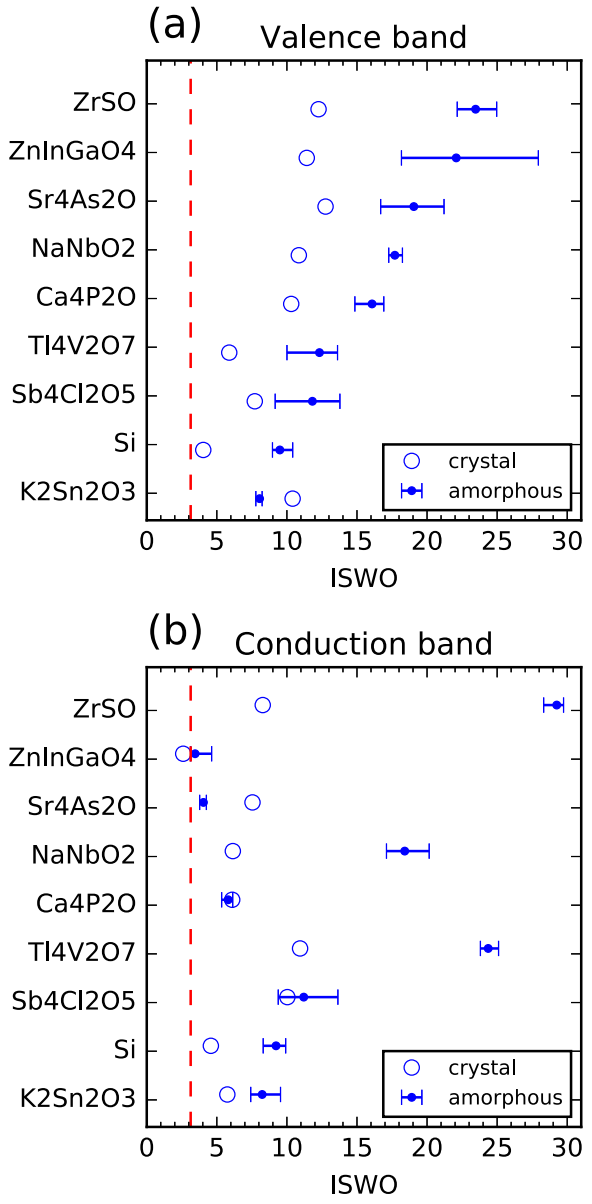

FIG. 10. Comparison of the ISWO values computed for (a) the valence and (b) the conduction bands of crystalline and amorphous phases of a selection of promising *p*-type oxides candidates (ZrOS, Sr_4As_2O, $NaNbO_2$, Ca_4P_2O, $Sb_4Cl_2O_5$, $Tl_4V_2O_7$, $K_2Sn_2O_3$). For each oxide, three different amorphous models containing a different number of atoms have been built and the averaged ISWO is provided. The error bars provide the lowest and highest values obtained for each material. For comparison purpose, the results obtained for three models of amorphous silicon and 13 models of *a*-IGZO (Fig. 8) are also provided. The red dashed lines corresponds to the lowest ISWO value obtained for the conduction band of the different *a*-IGZO models.

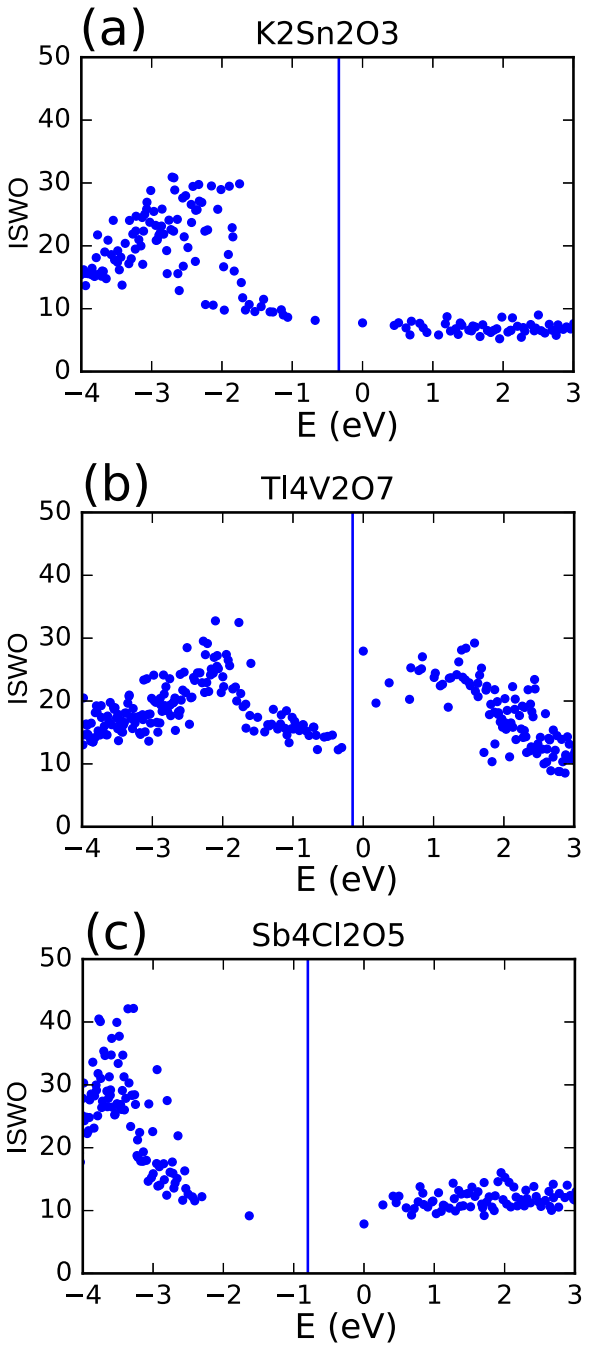

FIG. 11. Evolution of the ISWO in function of the energy for (a) $K_2Sn_2O_3$, (b) $Tl_4Cl_2O_5$, and (c) $Sb_4Cl_2O_5$. The vertical lines set the Fermi levels in the structures.

of crystalline *p*-type oxide candidates recently proposed by Hautier *et al.* [12], namely, ZrOS, Sr_4As_2O, $NaNbO_2$, Ca_4P_2O, $Sb_4Cl_2O_5$, $Tl_4V_2O_7$, and $K_2Sn_2O_3$. For each candidate, we built three different amorphous models whose number of atoms varies between 84 and 156.

Since there is no absolute reference for an ISWO value, we compare the top of the valence band of *p*-type oxide candidates with the ones of the conduction band of *a*-IGZO and of the band edge states of *a*-Si, for which the mobilities are known. Whenever the value computed for the valence band of the oxide candidate is similar, or lower, to the one of the conduction band of *a*-IGZO, the amorphous semiconductor is expected to show a similar or an improved hole mobility with respect to the electron mobility of *a*-IGZO. The results are shown in Fig. 10. The valence band ISWO values of all the candidates are relatively large compared to the one of the conduction band of *a*-IGZO. Only one candidate ($K_2Sn_2O_3$) is scoring

slightly better than *a*-Si. The former ISWO value is, however, twice as large as the one for the conduction band of *a*-IGZO. These results suggest that although these new candidates own promising effective mass in their crystalline phase, their properties are severely degraded upon amorphization and none of them is likely to be a high-mobility *p*-type amorphous semiconductor.

Interestingly, the ISWO value of the valence band of $K_2Sn_2O_3$ in its amorphous phase is lower than the one in its crystalline phase. This suggests that, in the valence band, the atoms interact on average more strongly together than in the crystalline phase. A more detailed analysis reveals that this variation arises from the increase of the Sn contribution to the wave function of the top of the valence band: in the crystalline phase, the Sn contribution is 1.6 times the one of oxygen, while in the amorphous one, the ratio doubles to reach 3.4. As Sn orbitals are more delocalized than the oxygen ones, the atomic interactions in these states are improved, which decreases the ISWO value. The effect can also be further analyzed by decomposing the ISWO values based on the type of atomic interactions: In the crystalline phase, the ISWO value of the top of the valence band is dominated by the Sn-O interaction (with a contribution of 49%), followed by the Sn-Sn interaction (30%) and the Sn-K interaction (19%). This radically changes in the amorphous phase, where the Sn-Sn interaction dominates with a contribution of 76% versus 11% and 12% for the Sn-O and Sn-K ones. The value of the ISWO hence increases in the amorphous phase thanks to the improvement of the Sn-Sn interactions at the top of the valence band.

Unfortunately, these valence band states remain dominated by *p* orbitals. These are directional, and their interaction degrades when the structure is amorphized. This stands in contrast to the case of the conduction band of *a*-IGZO, in which the states of interest are dominated by highly delocalized *s* orbitals, which are rather insensitive to amorphization. Interestingly, for the bottom of the conduction band, two candidates (Sr_4As_2O and Ca_4P_2O) show ISWO values remarkably close to the *a*-IGZO one, suggesting an electron mobility almost comparable to that of *a*-IGZO. They are nonetheless larger, implying that these candidates likely have a limited technological value.

Although the ISWO value of the top of the valence band of $K_2Sn_2O_3$ is not significantly better than the one of *a*-Si, its distribution in the states buried deeper in the valence bands is improved as shown in Fig. 11(a), where a linear decrease of the ISWO value is observed close to the valence band edge. The variations induced by the models (Fig. 10) are also the weakest among all the amorphous systems. Similarly to $K_2Sn_2O_3$, the ISWO values of the top of the valence band for $Tl_4Cl_2O_5$ and $Sb_4Cl_2O_5$ also tend to decrease close to the gap edges, as evidenced in Figs. 11(b) and 11(c). The ISWO distribution in these materials is unfortunately larger and more scattered than for $K_2Sn_2O_3$ (Fig. 10). Consequently, out of the seven oxides studied, $K_2Sn_2O_3$ is the most robust candidate to maintain its properties upon amorphization and could potentially show some *p*-type conductivity. Unfortunately, the ISWO signature is rather similar to the one obtained for *a*-Si, implying that the hole charge carrier mobility should be rather similar to the electron mobility of *a*-Si.

VI. CONCLUSION

We developed a methodology to evaluate the ability of an electronic state to transport a charge carrier in a disordered atomic phase. The proposed "inverse state weighted orbital" (ISWO) method captures, for a given electronic state, the extent and the strength of the interaction between their constitutive orbitals in electronic states. The ISWO values are independent of the number of atoms used in the model and on the nature of the basis set used.

We show that amorphous materials whose valence and conduction bands have low ISWO values are the most likely to possess a high charge carrier mobility. Based on this approach, we investigated the evolution of the properties of a set of crystalline and amorphous semiconducting oxides recently proposed for their potential to display *p*-type semiconducting characteristics. It is found that upon amorphization, only one of the candidates proposed ($K_2Sn_2O_3$) keeps a promising ISWO signature. The amorphous phase of $K_2Sn_2O_3$ is expected to present a *p*-type mobility similar to the one reported for electrons in *a*-Si, remaining at least one order of magnitude lower than the electron mobility of *a*-IGZO.

[1] J. Yeon Kwon and J. Kyeong Jeong, Semicond. Sci. Technol. **30**, 024002 (2015).

[2] J. S. Park, W.-J. Maeng, H.-S. Kim, and J.-S. Park, Thin Solid Films **520**, 1679 (2012).

[3] I. Sullivan, B. Zoellner, and P. A. Maggard, Chem. Mater. **28**, 5999 (2016).

[4] Z. Wang, P. K. Nayak, J. A. Caraveo-Frescas, and H. N. Alshareef, Adv. Mater. **28**, 3831 (2016).

[5] E. Fortunato, P. Barquinha, and R. Martins, Adv. Mater. **24**, 2945 (2012).

[6] K. Kaneko, N. Inoue, S. Saito, N. Furutake, and Y. Hayashi, in *VLSI Technology (VLSIT), 2011 Symposium on* (IEEE, Piscataway, NJ, 2011), pp. 120–121.

[7] L. J. Chi, M. J. Yu, Y. H. Chang, and T. H. Hou, IEEE Electron Device Lett. **37**, 441 (2016).

[8] Y. Ogo, H. Hiramatsu, K. Nomura, H. Yanagi, T. Kamiya, M. Hirano, and H. Hosono, Appl. Phys. Lett. **93**, 032113 (2008).

[9] J. A. Caraveo-Frescas, P. K. Nayak, H. A. Al-Jawhari, D. B. Granato, U. Schwingenschlögl, and H. N. Alshareef, ACS Nano **7**, 5160 (2013).

[10] P. Drude, Ann. Phys. **306**, 566 (1900).

[11] P. Drude, Ann. Phys. **308**, 369 (1900).

[12] G. Hautier, A. Miglio, G. Ceder, G.-M. Rignanese, and X. Gonze, Nat. Commun. **4**, 2292 (2013).

[13] W. Setyawan, R. M. Gaume, S. Lam, R. S. Feigelson, and S. Curtarolo, ACS Comb. Sci. **13**, 382 (2011).

[14] G. Hautier, A. Miglio, D. Waroquiers, G. M. Rignanese, and X. Gonze, Chem. Mater. **26**, 5447 (2014).

[15] N. Mott, Philos. Mag. **19**, 835 (1969).

[16] V. Ambegaokar, B. I. Halperin, and J. S. Langer, Phys. Rev. B **4**, 2612 (1971).
[17] V. Stehr, J. Pfister, R. F. Fink, B. Engels, and C. Deibel, Phys. Rev. B **83**, 155208 (2011).
[18] R. A. Marcus, J. Chem. Phys. **24**, 966 (1956).
[19] R. A. Marcus, Rev. Mod. Phys. **65**, 599 (1993).
[20] P. Friederich, F. Symalla, V. Meded, T. Neumann, and W. Wenzel, J. Chem. Theory Comput. **10**, 3720 (2014).
[21] C. Sutton, J. S. Sears, V. Coropceanu, and J.-L. Brédas, J. Phys. Chem. Lett. **4**, 919 (2013).
[22] I. Yavuz, B. N. Martin, J. Park, and K. Houk, J. Am. Chem. Soc. **137**, 2856 (2015).
[23] A. de Jamblinne de Meux, G. Pourtois, J. Genoe, and P. Heremans, J. Phys.: Condens. Matter **29**, 255702 (2017).
[24] N. C. Murphy, R. Wortis, and W. A. Atkinson, Phys. Rev. B **83**, 184206 (2011).
[25] C. Hartwigsen, S. Goedecker, and J. Hutter, Phys. Rev. B **58**, 3641 (1998).
[26] J. VandeVondele and J. Hutter, J. Chem. Phys. **127**, 114105 (2007).
[27] S. Goedecker, M. Teter, and J. Hutter, Phys. Rev. B **54**, 1703 (1996).
[28] M. Krack, Theor. Chem. Acc. **114**, 145 (2005).
[29] J. P. Perdew, K. Burke, and M. Ernzerhof, Phys. Rev. Lett. **77**, 3865 (1996).
[30] A. de Jamblinne de Meux, G. Pourtois, J. Genoe, and P. Heremans, J. Phys. D: Appl. Phys. **48**, 435104 (2015).
[31] Y. Youn, Y. Kang, and S. Han, Comput. Mater. Sci. **95**, 256 (2014).
[32] A. Jain, S. P. Ong, G. Hautier, W. Chen, W. D. Richards, S. Dacek, S. Cholia, D. Gunter, D. Skinner, G. Ceder *et al.*, APL Mater. **1**, 011002 (2013).
[33] S. P. Ong, W. D. Richards, A. Jain, G. Hautier, M. Kocher, S. Cholia, D. Gunter, V. L. Chevrier, K. A. Persson, and G. Ceder, Comput. Mater. Sci. **68**, 314 (2013).
[34] S. P. Ong, S. Cholia, A. Jain, M. Brafman, D. Gunter, G. Ceder, and K. A. Persson, Comput. Mater. Sci. **97**, 209 (2015).
[35] R. S. Mulliken, J. Chem. Phys. **23**, 1833 (1955).
[36] P. Markos and C. M. Soukoulis, *Wave Propagation: From Electrons to Photonic Crystals and Left-Handed Materials* (Princeton University, Princeton, NJ, 2008).
[37] M. Nisoli and S. E. Esculapio, *Semiconductor Photonics: Principles and Applications* (Società Editrice Esculapio, Bologna, Italy, 2016).
[38] K. Momma and F. Izumi, J. Appl. Crystallogr. **44**, 1272 (2011).
[39] R. Hoffmann, *Solids and Surfaces: A Chemist's View of Bonding in Extended Structures* (Wiley- VCH, New York, 1988).
[40] K. Nomura, H. Ohta, A. Takagi, T. Kamiya, M. Hirano, and H. Hosono, Nature (London) **432**, 488 (2004).
[41] P. Heremans, A. K. Tripathi, A. de Jamblinne de Meux, E. C. P. Smits, B. Hou, G. Pourtois, and G. H. Gelinck, Adv. Mater. **28**, 4266 (2016).
[42] T.-C. Fung, C.-S. Chuang, C. Chen, K. Abe, R. Cottle, M. Townsend, H. Kumomi, and J. Kanicki, J. Appl. Phys. **106**, 084511 (2009).
[43] Y. Pan, F. Inam, M. Zhang, and D. A. Drabold, Phys. Rev. Lett. **100**, 206403 (2008).
[44] J. Dong and D. A. Drabold, Phys. Rev. Lett. **80**, 1928 (1998).
[45] I. I. Fishchuk, A. Kadashchuk, A. Bhoolokam, A. de Jamblinne de Meux, G. Pourtois, M. M. Gavrilyuk, A. Köhler, H. Bässler, P. Heremans, and J. Genoe, Phys. Rev. B **93**, 195204 (2016).
[46] T. Kamiya, K. Nomura, and H. Hosono, J. Disp. Technol. **5**, 273 (2009).